Jovic, V., Rettie, A. J. E., Singh, V. R., Zhou, J., Lamoureux, B., Buddie Mullins, C., Bluhm, H., Laverock, J., & Smith, K. E. (2016). A soft X-ray spectroscopic perspective of electron localization and transport in tungsten doped bismuth vanadate single crystals. *Physical Chemistry Chemical Physics*, *18*(46), 31958-31965. https://doi.org/10.1039/c6cp04526j

A soft x-ray spectroscopic perspective of electron localization and transport in tungsten doped bismuth vanadate single crystals

Vedran Jovic,[a,b] Alexander J. E. Rettie,[c] Vijay R. Singh,[d] Jianshi Zhou,[e] Bethany Lamoureux,[d] Charles B. Mullins,[c,e] Hendrik Bluhm,[f] Jude Laverock,[d,g] Kevin E. Smith.[a,b,d]*

[a] School of Chemical Sciences and Centre for Green Chemical Sciences, The University of Auckland, Auckland 1142, New Zealand.

[b] The MacDiarmid Institute for Advanced Materials and Nanotechnology, Victoria University of Wellington, Wellington 6140, New Zealand.

[c] McKetta Department of Chemical Engineering, The University of Texas at Austin, Austin, Texas 78712, USA.

[d] Department of Physics, Boston University, Boston, MA 02215, USA.

[e] Texas Materials Institute, The University of Texas at Austin, Austin, Texas 78712, USA.

[f] Chemical Sciences Division, Lawrence Berkeley National Laboratory, Berkeley, CA 94720, USA.

[g] School of Physics, H.H. Wills Physics Laboratory, Tyndall Avenue, University of Bristol, Bristol, BS8 1TL, United Kingdom.

Abstract: Doped $BiVO_4$ is a promising photoelectrochemical water splitting anode, whose activity is hampered by poor charge transport. Here we use a set of x-ray spectroscopic methods to probe the nature of localized electron states in W:$BiVO_4$ and variations in the electronic structure along the crystal axes related to the materials conductivity anisotropy. We verify that tungsten substitutes as W^{6+} for V^{5+} in $BiVO_4$. This results in the presence of inter-band gap states related to electrons at V^{4+} sites of *e* symmetry. The energetic position of the states in the

band gap suggest that they are highly localized and may act as recombination centres. Polarization dependent x-ray absorption spectra reveal anisotropy in the electronic structure between the *ab*-plane and *c*-axis. Results show the superior hybridization between V 3*d* and O 2*p* states, higher V wavefunction overlap and broader conduction bands in the *ab*-plane than in the *c*-axis. These insights into the electronic structure are discussed in the context of existing experimental and theoretical reports regarding charge transport in $BiVO_4$.

INTRODUCTION

Monoclinic scheelite bismuth vanadate (*ms*-$BiVO_4$), is a promising metal oxide for use as an anode in photoelectrochemical (PEC) water splitting. This is due to its favourable band energetics, ~2.5 eV band gap, and encouraging solar conversion efficiencies.[1,2] Advances in the PEC activity of $BiVO_4$ stem from studies dedicated to finding suitable co-catalysts capable of stabilizing the material in aqueous environments and improving charge carrier transport.[3-5] However, the low conductivity of *ms*-$BiVO_4$, due to unfavourable electron localization ('small-polaron' formation), limits its water oxidation efficiency.[6,7] Thus, continued efforts aimed at understanding the nature of electron trap states and poor carrier transport in doped and pure $BiVO_4$ may aid in the material's further development for PEC water splitting.

In pristine $BiVO_4$, a polaron is proposed to form when the poorly screened electric field of an electron distorts the crystal lattice, which in turn creates a trapping potential for the carrier (i.e. electron-phonon coupling).[13] This polaron quasiparticle 'hops' through the lattice, drastically reducing mobility. Various groups have attempted to improve the bulk conductivity of $BiVO_4$ by molybdenum (Mo) or tungsten (W) doping.[3,9] Despite an increase in electron density and an improved photoresponse, Abdi *et al*. showed that doping increased charge

recombination rates due to the introduction of intermediate-depth donor defects as charge carrier traps.[5,9] To probe the nature and behaviour of excess electrons in 'doped' $BiVO_4$, DFT+U hybrid computational methods have been applied.[7,10] Excess electrons were predicted to localize at V $3d_z^2$ sites, which resulted in the formation of inter-band gap small-polaron states. The data was consistent with electronic transport measurements indicating that despite an increase in the PEC activity of $BiVO_4$ with doping, the electronic mobility remains low, yet consistent with small-polaron hopping, $\sim 10^{-4}$ cm^2 V^{-1} s^{-1} (upper limit in the small-polaron hopping regime is ~0.1-1 cm^2 V^{-1} s^{-1}).[6] Intriguingly, DFT verified that the small polaron hopping activation energy (E_a) relies on the electronic coupling of the initial and final states of the hop, possibly indicating that electron mobility may increase as vanadium wavefunction overlap improves.[7] Coupled with previous results revealing a conductivity anisotropy ratio of 2.3 between the *ab*-plane and *c*-plane in M:$BiVO_4$ (where M = W or Mo),[8] the theoretical and experimental results suggest that the lattice structure and electron localization play a strong role in the material's bulk conduction.

Both electronic transport studies and DFT+U hybrid computational methods have been used to understand the electronic structure and its influence on the nature of charge transport in *ms*-$BiVO_4$. This understanding can be expanded by probing the materials electronic band structure from an x-ray spectroscopic perspective. Here, we use resonant photoemission (RPES), x-ray absorption (XAS) and emission spectroscopies (XES) to probe the; i) local environment of dopant species; ii) the nature of localized electron states and; iii) the structural driving forces manifesting in the low charge carrier mobility's in W doped $BiVO_4$ single crystals. The study is a timely extension of earlier electron transport work on M:$BiVO_4$ single crystals showing anisotropic small-polaron conduction.[6,8] The ability of x-rays to show changes

in the electronic structure along the crystal axes may allow us to shed further light on the structural aspects influencing carrier mobility.

EXPERIMENTAL METHODS

Single crystals of 0.3% W doped $BiVO_4$ (and 0.6 % Mo:$BiVO_4$) were grown by a floating zone method in an optical image furnace at the University of Texas at Austin.[6] Information regarding the crystal growth procedures, structural characterization, quantitative analysis of doping percentages along with results of PEC performance and electronic transport measurements were comprehensively reported in references 6 and 8. Single crystal boules were cleaved *ex-situ* to give mirror-like faces with the *c*-axis perpendicular to the surface. PES measurements were performed at beamline 11.0.2 of the Advanced Light Source, Lawrence Berkeley National Laboratory.[12,13] Spectra were calibrated against the 4f peaks of metallic gold. RPES data were collected by initially recording an XAS spectrum in the total electron yield (TEY) mode at the V $L_{3,2}$ edge and subsequently tuning the incident x-ray energy to a particular feature in the spectrum. The ultra-high vacuum chamber base pressure was $<5\times10^{-9}$ Torr for measurements. XAS, XES and resonant inelastic x-ray scattering (RIXS) data were collected at ALS beamline 8.0.1. XAS was collected in both the surface sensitive (~10 nm) TEY mode, and in the bulk sensitive (~100 nm) total fluorescence yield (TFY) mode. The beamline energy resolution for these measurements was 0.3 eV at FWHM. The incident photon polarization was direct to be either parallel to the *ab*-plane (referred to as '$E_{\|ab}$') or parallel to the *c*-axis ('$E_{\|c}$'). Spectra were calibrated with reference to the Ti *L*- and O *K*-edge of rutile TiO_2. O *K*-edge XES data (with a spectral resolution of 0.70 eV) were calibrated with reference to the $L_{\alpha1,2}$ and $L_{\beta1}$ second order emission lines of Zn foil. The spectra were recorded with a 90° scattering geometry, and the incident x-rays were at 45° relative to the surface normal of

the sample. The sampling depth of the XES measurements is estimated to be close to the TFY sampling depth.

RESULTS AND DISCUSSION

Figure 1 (a) shows valence band (VB) photoemission spectra for 0.3% W:$BiVO_4$ excited with incident x-ray energies of 630 eV and 350 eV (probing slightly different depths in the vicinity of the surface, as discussed below).[11] Note that survey and O 1*s* spectra collected after 300 ºC heat treatment in a 1×10^{-6} Torr oxygen atmosphere are shown in Supplementary Fig. 1 (a)-(b). Based on formerly determined band gap energies of 2.5-2.7 eV, the E_F in Fig. 1(a) is closer to the conduction band (CB) onset (indicating that the sample is *n*-type).[6,11] Briefly, the $BiVO_4$ VB density of states contains strong contributions from O 2*p* states extending to ~6 eV below the E_F, along with Bi 6*p* and V 3*d* states at ~8-4 eV (green in Fig. 1 (a)).[14,15] This heavy O 2*p* character offers resistance to oxidation and large over-potentials.[16] Bi^{3+} 6*s* electron lone pairs interact with O 2*p* states, forming antibonding states at the top of the VB. The antibonding destabilization is reduced by a slightly distorted (and energetically favorable) monoclinic scheelite structure of $BiVO_4$, allowing for otherwise symmetrically forbidden mixing between Bi 6*s* and Bi 6*p* states.[14,17] The spectra of W:$BiVO_4$ at 630 eV and 350 eV (resulting in inelastic mean free paths of ~14 and 9 Å, respectively) show a peak above the VB maximum (highlighted in red at ~1.8 eV in Fig. 1 (a)), which was otherwise absent in the VB spectra of pure $BiVO_4$ (shown at the inset of Fig. 1 (a)). The existence of this state can also be observed in 0.6 % Mo doped $BiVO_4$ (Supplementary Fig. 2). In particular, at hν = 350 eV (dashed red line in Fig. 1 (a)), a feature develops at the Fermi level and extends to ~0.5 eV below, in close agreement with expectations from electronic transport data and consistent with the existence of shallow electron donor levels.[8] The feature possibly arises due to the presence

of oxygen vacancies and has been proposed to result in a dispersive metallic state at the Fermi level – in close vicinity to the CB. In TiO_2, it has been suggested that at above 60 K, such electrons thermally excite into the CB, resulting in more metallic-like transport. At lower temperatures, the increase of resistivity shows that the states are polarons.[18,19] Similar features to the ones seen at 1.8 eV were also seen in CeO_2 upon reduction of Ce^{4+} to Ce^{3+} and assigned to localized electrons in a narrow Ce 4f electronic state in the band gap.[20] However, electron doping by substitution of M^{6+} for V^{5+} presents a challenge in discerning inter-band gap features between alloying induced defect states, polarons and oxygen vacancies, all of which could increase V^{4+} concentrations. The origin and the nature of the inter-band gap states are explored in greater detail in the discussion below.

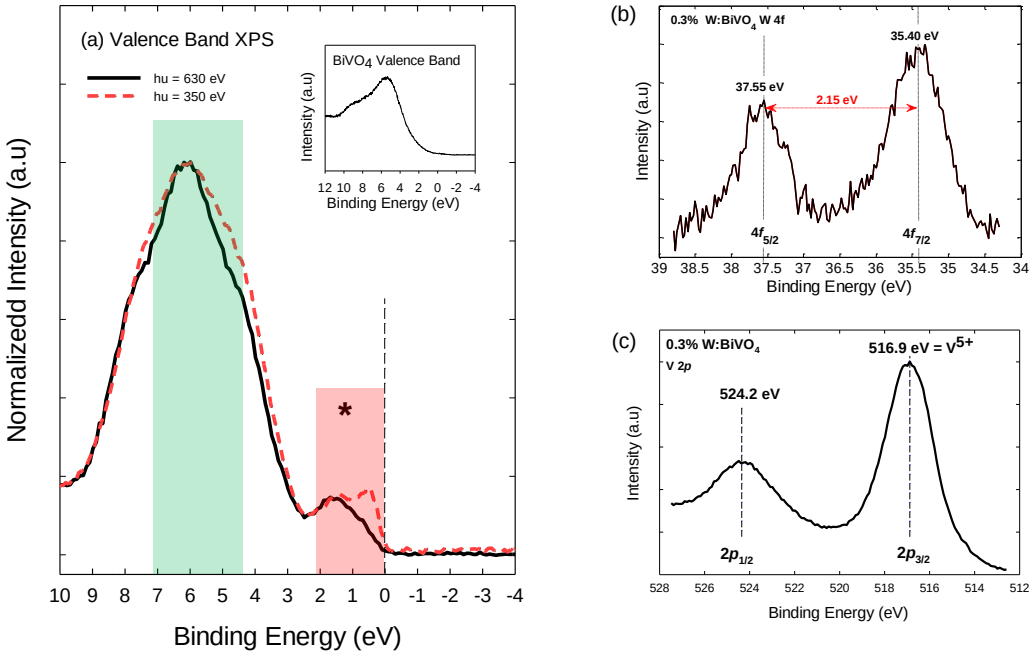

Figure 1. (a) Valence band PES for 0.3% W:$BiVO_4$, collected using an incident photon energy (hν) of 630 eV and 350 eV. Electron trap states at ~1.8 eV are seen in both spectra (highlighted in red). At hν = 350 eV (dashed red line), a feature develops at the Fermi level and extends to ~0.5 eV below. **(b)** W 4f core level PES for 0.3% W:$BiVO_4$. The binding energies of the SOS $4f_{7/2}$ and $4f_{5/2}$ features (35.40 eV and 37.55 eV, respectively) are characteristic of a W^{6+} oxidation state. **(c)** V 2*p* core level PES for the 0.3% W:$BiVO_4$ single crystal.

The floating zone growth method, which was used to fabricate the M:$BiVO_4$ single crystals, permitted final doping concentrations of 0.3% for W and 0.6% for Mo, as determined by inductively coupled plasma mass spectrometry (ICPMS).[6] These low doping percentages made x-ray analysis of the W and Mo bonding environments challenging with conventional techniques. Here we attempted to probe the nature of the dopant species in the $BiVO_4$ lattice using high resolution PES. Tungsten 4f core level PES of 0.3% W:$BiVO_4$ is shown in Fig. 1 (b). The spectrum is dominated by W $4f_{7/2}$ and W $4f_{5/2}$ spin orbit split (SOS) peaks at ~35.40 eV and ~37.55 eV (SOS = 2.15 eV) in a 4:3 peak height ratio, typical for that of f-orbitals. The binding energy of the 4f peaks suggest that W is in the 6+ oxidation state and presumably substitutes for the V^{5+} site, forming V^{4+} ions and contributing to the existence of the inter-band

gap electronic states (in Fig. 1 (a)) on account of electron donation.[21,22] The existence of V^{4+} states in W:$BiVO_4$ was probed by V 2*p* core level XPS (Fig. 1 (c)). V $2p_{3/2}$ and $2p_{1/2}$ spin orbit split (SOS) peaks at 516.9 and 524.0 eV (SOS = 7.1 eV) in a 2:1 peak ratio, are typical for the V^{5+} oxidation state. The absence of a V^{4+} shoulder at ~515.7 eV is not unexpected on account of the low W doping (0.3 at.%, as determined by both XPS and ICPMS).[6] Coupled with the VB spectra in Fig. 1 (a) and Supplementary Fig. 2, this analysis tentatively suggests that the existence of inter-band gap states is partly due to the replacement of V^{5+} with W^{6+} (or Mo^{6+} - shown below). However, electron doping (due to oxygen off-stoichiometry's from growth or x-ray beam damage) is likely. Substitution of W^{6+} for V^{5+} is consistent with DFT calculations used by Ding *et al*. to simulate the effects of doping (namely Mo) on the physicochemical properties of $BiVO_4$.[23] The impurity formation energy for Mo at the V^{5+} (as Mo^{6+}) and Bi^{3+} (as Mo^{3+}) sites (0.53 eV and 2.79 eV, respectively) shows that the dopant likely substitutes for V. Due to the similar atomic radii between Mo and V, the calculated structures did not show major lattice distortions (also evidenced by our earlier V *L*- and O *K*-edge XAS showing no change following W or Mo doping).[11] We also show the substitution of Mo^{6+} for V^{5+} through Mo $M_{3,2}$-edge XAS spectra from a 0.6% Mo:$BiVO_4$ single crystal (Supplementary Fig. 3). The M_3 edge (Mo $3p_{3/2} \rightarrow$ Mo *d*-state transition) appears to further split into the *e* (396.9 eV) and t_2 (398 eV) states, separated by 2.1 eV due to the tetrahedral crystal field, suggesting that Mo occupies the V^{5+} site.[24-26] Thus, the peak positions and spectral shape at the M_3 edge are consistent with an Mo^{6+} ($4d^0$) oxidation state. Note that the melt growth technique produces large boules of crystalline material, from which the crystals were cut. As the samples were obtained from the boules bulk, surface segregation is unlikely. Accordingly, it is assumed that doping in the single crystals is homogeneous (i.e., no surface segregation takes place).

Resonant PES (RPES) offers the ability to tune the x-ray energy to that of a core level, allowing us to probe the site specific occupied partial density of states (pDOS) near the Fermi level. Thus, RPES is used to examine the nature and orbital symmetry of the electron trap states formed in $BiVO_4$ by electron doping. Figure 2 (a) displays RPES for 0.3% W:$BiVO_4$ at various excitation energies along the V $L_{3,2}$ absorption edge (Fig. 2 (b)). If we briefly first consider the main features of the V *L*-edge in Fig. 2 (b), the spectrum is dominated by the L_3 edge (excitation from V $2p_{3/2}$ to V 3d states) and L_2 edge (excitation from V $2p_{1/2}$ to V 3*d* states).[11] The regions are separated by 6.65 eV due to the spin-orbit coupling of the 2*p* core-hole. The L_3 edge further splits into two regions; the *e* (516.3 eV) and t_2 (518.5 eV) states, separated by 2.20 eV on account of the tetrahedral crystal field. In Fig. 2 (a), the intensification of the electron trap state at 1.8 eV as the incident photon energy moves across both the V L_3 and L_2 edges is clear. This observation was also seen in the Mo:$BiVO_4$ crystal (not shown here). The dependence of the trap state peak intensity on points of resonance corresponding to orbitals of particular symmetry at both edges is highlighted more specifically in Fig. 2 (c) and discussed below in conjunction with Fig. 2 (d).

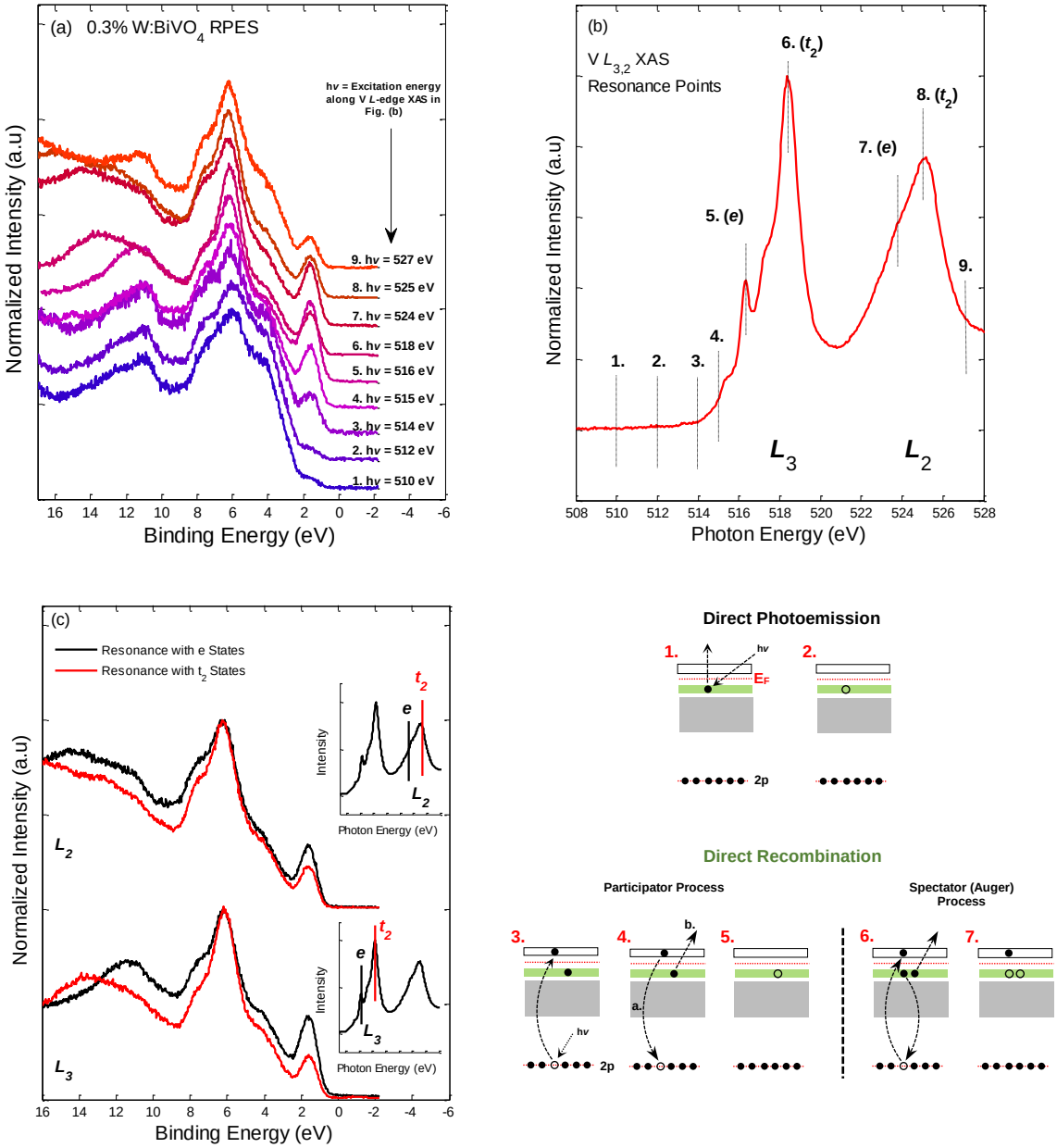

Figure 2. (a) Valence band resonant photoemission spectra for 0.3% W:$BiVO_4$ recorded at x-ray energies corresponding to absorption features at the V $L_{3,2}$ absorption edge. **(b)** Selected points of resonance along the V $L_{3,2}$ absorption edge for the collection of VB spectra shown in (a). **(c)** VB RPES spectra collected at incident photon energies corresponding to absorption features into orbitals of *e* and t_2 symmetry at the L_3 and L_2 edges. **(d)** Schematic representation of direct photoemission and direct recombination which collectively describe the enhancement of a particular VB feature using resonant photoemission.

Figure 2 (c) shows VB RPES collected using x-ray energies corresponding to the *e* peak (black) and t_2 peaks (red) at both the L_3 and L_2 edges. The intensity of the 1.8 eV trap state is

highest when resonating with states of *e* symmetry at the L_3 or L_2 edge. This can be understood in terms of the constructive interaction of two parallel processes, direct photoemission and direct recombination, arising between V 2*p* core states and (un)occupied V 3*d* states (described in conjunction with the schematics in Fig. 2 (d)).[27] In direct photoemission (Schematics 1 and 2 in Fig. 2 (d)), resonance with an *L*-edge absorption feature (and concurrently with a V 2*p* core level) results in the emission of an electron from an occupied V 3*d* level ($2p^6 3s^2 3p^6 3d^x + h\nu \rightarrow 2p^6 3s^2 3p^6 3d^{x-1} + e^-$), producing a continuous photoemission spectrum. Resonance with the 2*p* core level also means that the above step is accompanied by a '*participator*' type direct recombination process (depicted in Schematics 3 to 5). Here, the resonant photon energy promotes a 2*p* core electron to an empty conduction state (Schematic 3), producing a hole in the 2*p* level ($2p^6 3s^2 3p^6 3d^x + h\nu \rightarrow 2p^5 3s^2 3p^6 3d^{x+1}$). Next, the electron promoted to the conduction state recombines with the 2*p* core hole (depicted as Step 'a.' in Schematic 4), releasing energy ($2p^5 3s^2 3p^6 3d^{x+1} \rightarrow 2p^6 3s^2 3p^6 3d^x + h\nu$). This energy ejects a valence electron from the 3*d* band ($2p^6 3s^2 3p^6 3d^x \rightarrow 2p^6 3s^2 3p^6 3d^{x-1}$) (depicted in Step 'b.' in Schematic 4). As the final states in the direct photoemission and participator type direct recombination steps are equivalent (i.e. Schematics 2 and 5), the ejected electrons have equal kinetic energies. Thus, the intensity of the VB feature, related with the molecular orbital to which the x-ray energy was tuned, is enhanced. The participator type direct recombination process is characterized by the fact that the 1.8 eV photoemission feature retains the same binding energy as the x-ray energy varies (Fig. 2 (a)). A 'spectator' (Auger) type of direct recombination (Schematics 6-7) may also occur, and results in a different final state to direct PES. Here the emitted electrons energy relates to the energy difference between the final state VB hole and CB electron. Thus, the occurrence of this Auger process would be reflected by a binding energy shift of the 1.8 eV feature as the incident photon energy is varied - not seen here. Thus, the enhancement of the PES intensity is directly related to the participator direct recombination process. On this basis,

electron trap states are related with V 3*d* states of *e* symmetry. This is consistent with theoretical predictions of excess electrons occupying V $3d_z^2$ states in $BiVO_4$.[7] Thus, our experiments show that excess electrons created by M^{6+} doping or via the formation of oxygen vacancies, also create highly localized trap states deep within the band gap of $BiVO_4$.

Electron doping and the existence of inter-band gap trap states and polaron-like states in $BiVO_4$ were the subject of two recent studies using hybrid DFT methods.[7,10] The methods were employed due to issues of conventional DFT in accurately predicting charge localization. The charge localization was modelled by including a Hartree-Fock (HF) exchange[7] or a U_{eff} parameter[10] (which accounts for the Coulomb interaction, U, and the exchange parameter, J (i.e. $U_{\text{eff}} = U - J$)). Excess electrons were shown to reside at the V sites, resulting in reduction of V^{5+} to V^{4+}. The ensuing electron delocalization to the surrounding oxygen atoms and a weak structural distortion (due to V-O bond elongation) were linked specifically to small-polaron formation. This led to the presence of states in the band gap, whose position was shown to also depend on the degree of HF exchange or magnitude of U_{eff}. By comparison with experimentally measured properties (specifically the band gap energy and the small-polaron activation energy) these states were located closer to the CB minimum.

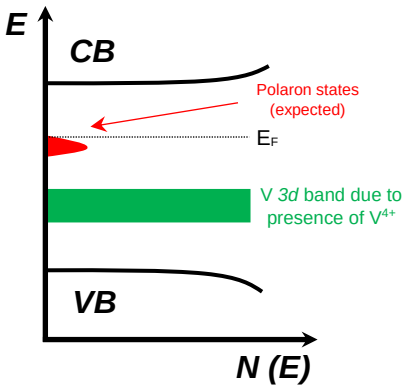

Figure 3. Energy diagram cartoon depicting possible trap states within the band gap in M^{6+} doped $BiVO_4$. Dashed horizontal line indicates the Fermi level and the solid green horizontal line represents shallow donor states due to M^{6+} doping.

Our VB PES and RPES show that a similar feature occupies the lower half of the band gap, far away from the conduction band maximum or valence band minimum. This is depicted by a schematic plot in Fig. 3. In this respect, the feature may signify the presence of deep trap states formed upon M^{6+} doping, distinct from the less localized nature of polaron states. Indeed, inter-gap trap states have been inferred by recent experimental studies of carrier dynamics in W:$BiVO_4$ thin films. Using time-resolved microwave conductivity, Abdi *et al*. observed rapid recombination of photo-generated carriers in W:$BiVO_4$ relative to $BiVO_4$, despite the fact that W:$BiVO_4$ shows higher photocurrents (consistent with our observations from M:$BiVO_4$).[5,9] The authors proposed that this result was due to inter-gap traps related to W^{6+} doping or a related defect.[9] Recently, Pattengale *et al*. performed transient absorption experiments on W:$BiVO_4$, proposing that tungsten doping resulted in a hole trap state near the VB, not unlike the feature we observed in our single crystals.[28] However, in contrast to Abdi *et al*., these authors reported reduced carrier recombination in their doped $BiVO_4$ films. Clearly, similar studies using single crystals with well-defined doping concentrations would be invaluable in fully assigning the nature of these states in the band gap and their effects on PEC performance.

X-ray absorption spectroscopy is a powerful tool for probing the electronic structure of materials, adept at revealing the unoccupied density of states (CB) of a semiconductor. In XAS, an electron is excited from a core level to an unoccupied CB state – a transition subject to dipole selection rules ($\Delta l = \pm 1$).[29] As touched upon in relation to Fig. 2, XAS at the V *L*-edge involves transitions from occupied V 2*p* states into unoccupied localized and delocalized V 3*d* states, which partially make-up the systems CB. In particular, XAS at the O *K*-edge (which we specifically probe below) involves transitions from occupied O 1*s* and unoccupied O 2*p* states. Hybridization between O 2*p* wave functions and neighboring V *d* electrons makes O *K*-edge XAS an ideal probe of the (hybridized) unoccupied states in the CB of a transition metal oxide. Furthermore, by rotating the polarization vector of the incident x-rays, XAS can also be used to couple electronic structure variations with observations of conductivity anisotropy in W:$BiVO_4$. Figure 4 (a) shows V $L_{3,2}$ XAS TFY spectra for the 0.3% W:$BiVO_4$ single crystal recorded with incident photon polarizations parallel to the *c*-axis ($E_{\|c}$, black) and parallel to the *ab*-plane ($E_{\|ab}$, green). The main features at the V $L_{3,2}$ edge (as labelled in the plot) were described in relation to Fig. 2 (b) and indicate the presence of V^{5+} in monoclinic scheelite structure of $BiVO_4$.[11,30] It is immediately clear that the L_3 edge, shows increased spectral weight at higher energies (just above the t_2 peak) for $E_{\|ab}$ relative to $E_{\|c}$. This observation is also evident at the L_2 edge. The equivalent spectra for the 0.6% Mo:$BiVO_4$ single crystal, omitted here for clarity purposes and shown in Supplementary Fig. 4 (a), were highly consistent with that of W:$BiVO_4$ in Fig. 4 (a). Collectively, these results suggest that the unoccupied vanadium bands (V pDOS) are broader for $E_{\|ab}$ than for $E_{\|c}$, particularly for the t_2 states. The broadening of the bandwidth in the *ab*-plane, discussed further below in context of the $BiVO_4$ electronic transport properties, results from the improved V wavefunction overlap in the *ab*-plane. Conversely, in the case of the *c*-axis, the states are narrower and experience less overlap. Furthermore, due to the non-dispersive nature of the V 2*p* core levels, an apparent weak increase in the SOS with

$E_{\|ab}$ can be seen in Fig 4 (a) (i.e. an increase in the energy separation between the t_2 states of the L_3 and L_2 edge). This is also evident, somewhat more so, in the equivalent spectra for the Mo:$BiVO_4$ (Supplementary Fig. 4 (a)). This observation also reflects the increased overlap of V wavefunctions in the *ab*-plane relative to the *c*-axis.

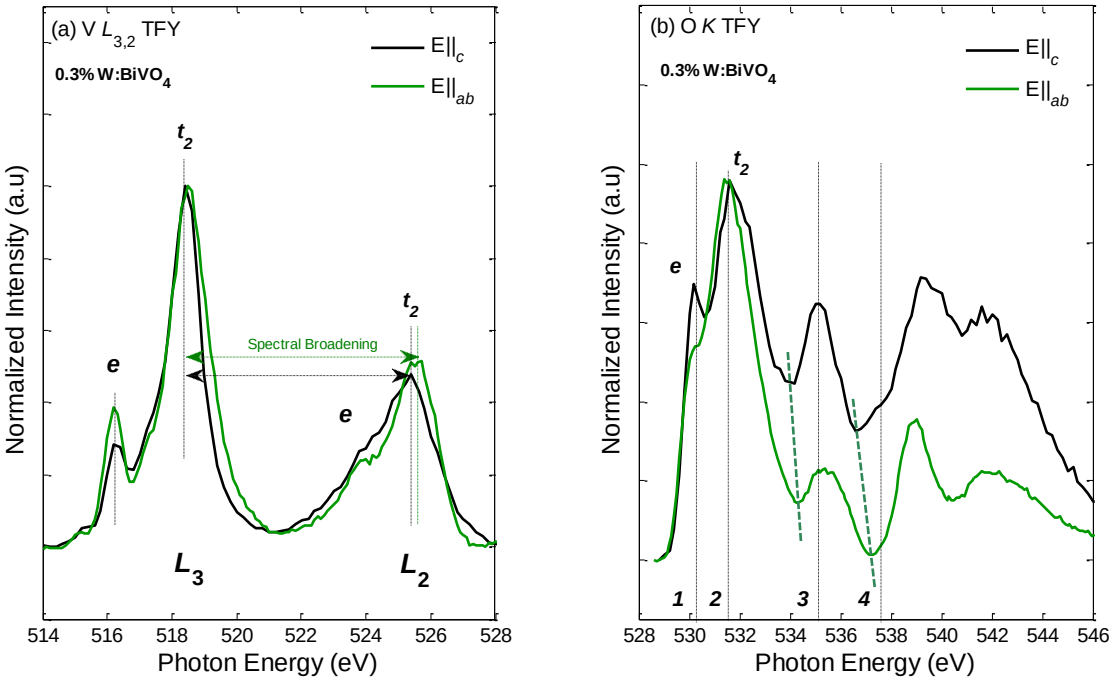

Figure 4. (a) V $L_{3/2}$ XAS TFY spectra for 0.3% W:$BiVO_4$ recorded with incident photon polarizations parallel (black) to the *c*-axis and parallel (green) to the *ab*-plane. **(b)** Corresponding O *K*-edge XAS TFY spectra for the 0.3% W:$BiVO_4$ single crystal recorded with incident photon polarizations parallel (black) to the *c*-axis and parallel (green) to the *ab*-plane.

Structurally similar observations to the ones described above can be made in Fig. 4 (b) which shows O *K*-edge XAS (TFY) for W:$BiVO_4$ at $E_{\|c}$ (black) and $E_{\|ab}$ (green). X-ray absorption at the oxygen *K* edge (i.e. $1s \rightarrow 2p$ transitions) is closely related to the unoccupied pDOS of transition metal oxides due to the hybridization of O 2*p* and V 3*d* states. The spectra for each polarization show characteristic features at 530.2 eV (1) and 531.8 eV (2), associated with hybridization of O 2*p* states with V *e* and t_2 states.[30] Feature 3 (Bi 6*p* states) shows

increased overlap with O 2*p* states along the *c*-axis, as is evidenced by its increased relative intensity with $E_{\|c}$. In contrast, for $E_{\|ab}$, the *e* and t_2 features are strongly enhanced. This observation also indicates that the hybridization between V 3*d* and O 2*p* states is strongly enhanced in the *ab*-plane relative to the *c*-axis. The results were consistent with the equivalent spectra for the 0.6% Mo:$BiVO_4$ single crystal (Supplementary Fig. 4 (b)). In addition to the above, the features are also marginally broader for $E_{\|ab}$, i.e. the minimum between feature 2 and feature 3 (shown by green dashed lines in Fig. 4 (b)) is at a higher photon energy for $E_{\|ab}$ than $E_{\|c}$. The same observation can be made for the minima between features 3 and 4 (also indicated in Fig. 4 (b)). This result, which is seen even more clearly in the spectra of M:$BiVO_4$ in Fig. 4 (b), points to a greater bandwidth in the *ab*-plane and is in agreement with observations made at the V L_3 and L_2 edges.

Collectively, the bandwidth broadening in the *ab*-plane relative to the *c*-axis, seen from our spectroscopic data, is in strong agreement with DC electrical conductivities being superior for motion in the *ab*-plane relative to the *c*-axis, as observed in earlier studies by Rettie *et al*., on these single crystals.[8] Specifically, the conductivity anisotropy ratio between the *ab*-plane and the *c*-axis was 2.3 ± 0.4.[8] The mechanism underlying the anisotropic conductivity was rationalized based on the $BiVO_4$ polar monoclinic scheelite structure, which consists of layered edge-sharing BiO_8 and VO_4 subunits separated by weakly bonded oxygen planes perpendicular to the *c*-direction (as shown in Supplementary Fig. 5 (a)).[6,8,30] In the structure, the resulting arrangement of V sites presents variations in 'Next-Nearest-Neighbor' (NNN) charge carrier hops between *ab*-plane and *c*-axis, and thus influences the conductivity anisotropy. This is explained below in conjunction with the schematic diagram in Supplementary Fig. 5 (b) (reproduced from Ref [8]). It was proposed that NNN hops in the *ab*-plane are around ~5.2 Å in length – NNN hops in the *ab*-plane are represented by the black zig-zag patterns in

Supplementary Fig. 5 (b). In contrast, NNN hops in the *c*-axis (represented by a blue line in Supplementary Fig. (5) (b)) are ~6.9 Å in length.[6,8] Coupled with the electronic transport data, this suggests that band of small-polaron states is wider for motion in the *ab*-plane than along the *c*-axis, as confirmed by our XAS data. This relatively 'weaker' wavefunction overlap of V-sites in the *c*-axis, seen in Fig. 4, may also affect the carrier hopping activation energy (E_a). In M:$BiVO_4$, it was proposed that small-polarons propagate by adiabatic hopping between V-sites.[6] E_a relies on the 'reorganization energy' (associated with the rearrangement of atomic sites to accommodate electron acceptance), and is predicted to decrease with higher electronic coupling between the initial and final sites of the hop.[7,16] Thus, the improved conductivity in the *ab*-plane may be a result of the superior V-wavefunction overlap decreasing E_a. The observations suggest that the modified growth/fabrication of $BiVO_4$ based photoanodes which promote the interaction of vanadium wavefunctions along the *c*-axis (conceivably through mechanical strain or chemically induced strain) may improve charge mobility and PEC activity. The effects of mechanical strain may be probed through the growth of epitaxial $BiVO_4$ films on substrates possessing a slight lattice mismatch to that of $BiVO_4$ (this may result in *c*-axis shrinkage or expansion depending on the orientation of the epitaxial film). Advances in carrier transport may also be achieved with higher electron doping levels (i.e. Mo^{6+}, W^{6+} or via oxygen vacancy formation) which effectively increase the overlap of polaronic wavefunctions.

We can also note in Fig. 4 (b) the weak appearance of feature 4 at ~537.3 eV, which only appears when $E_{\|c}$. The appearance of this feature is particularly evident in the spectra of Mo doped $BiVO_4$ (Supplementary Fig. 4 (b)). The site specific pDOS related to this feature has been probed by resonant XES (RXES), and we further probe the nature of this feature here.[11] In 'XES, the system is excited in an equivalent manner to XAS.[31] However, the measurement focuses on the fluorescent decay of valence band electrons which fill the core holes left behind

in the initial excitation process.[29] Thus, in a complimentary manner to XAS, XES measures the systems occupied partial density of states (the valence band). At the O *K*-edge, the fluorescent decay resulting from transitions between occupied O 2*p* valence band states to the O 1*s* core level is measured and provides a picture of the occupied oxygen partial DOS. This 'normal' XES process (where the initial excitation is achieved with x-ray energies well above the O *K*-absorption edge) yields an emission spectrum which is independent of the excitation energy. By resonantly exciting the system at an energy corresponding to a feature in the XAS spectrum (RXES), it is possible to measure the site-selective occupied pDOS.[31,32] Figure 5 shows O *K*-edge RXES for W:$BiVO_4$. Spectra were collected with photon energies of 537.3 eV (resonant with feature '4') and >550 eV (i.e. well above the absorption threshold). Resonance at 537.3 eV leads to a distinct enhancement of a low energy feature at 510.5 eV (1) associated with V $L_{\alpha\,1,2}$ emission (V 3*d* → V 2*p*), as well as the enhancement of feature (2) at 517.5 eV (~7 eV above the V $L_{\alpha\,1,2}$ feature). The separation in energy between features (1) and (2) is close to the SOS of the V L_3 and V L_2 absorption features in Fig. 4 (a) (~6.8 eV), and we tentatively assign the 517.5 eV peak to V L_β emission. The equivalent spectra for Mo:$BiVO_4$ are shown in Supplementary Fig. 6. We note that previously non-resonant XES data $BiVO_4$ attributed a similar feature at this energy to Bi 6*s* - O 2*p* states, which are expected from DFT calculations to be ~ 10 eV below the VBM (~ 517.5 eV in Fig. 5) and therefore overlap V L_β emission.[14,15] While we cannot exclude a contribution from Bi 6*s* states in our data, the simultaneous resonant enhancement of this feature together with V L_α emission in both compounds strongly suggests V L_β emission is predominantly responsible for this peak at the resonant energies chosen here. With this in mind, we associate the 537.3 eV CB feature [feature 4 in Fig. 4(b)] with unoccupied bulk V states. However, feature 1 experiences a slightly higher enhancement relative to feature 2 with resonance at 537.4 eV (in comparison to resonance at 550 eV). Thus contributions from Bi states at 517.5 eV cannot be discounted.

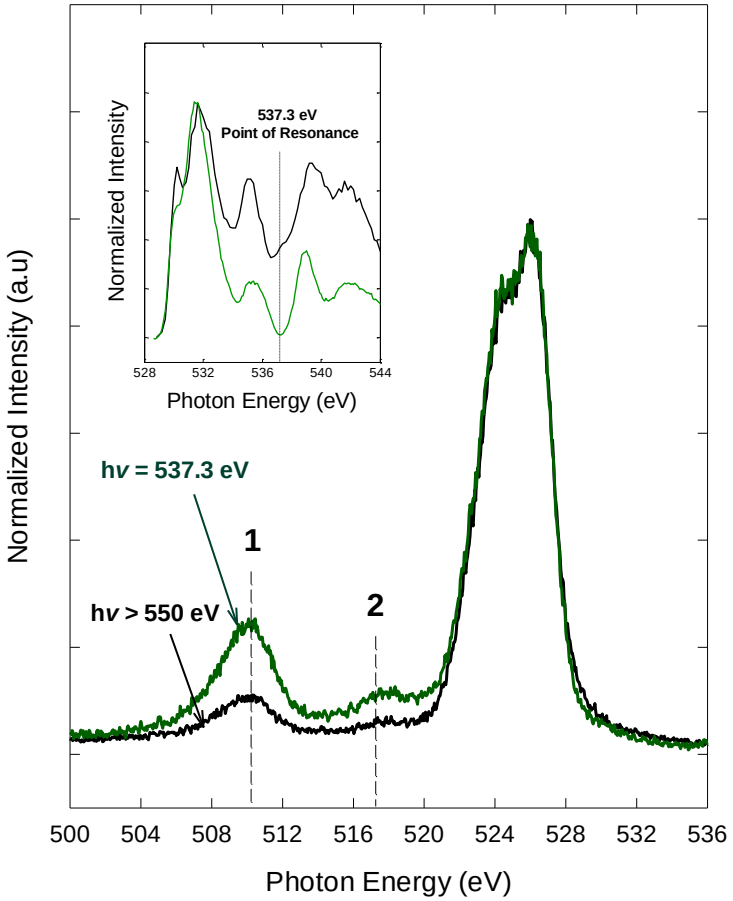

Figure 5. O *K*-edge RXES for 0.3% W:$BiVO_4$. Spectra were recorded following irradiation with incident photon energies of 537.3 eV and >550 eV.

CONCLUSIONS

This study employed a suite of soft x-ray spectroscopic methods to probe the nature of localized electron states in W:$BiVO_4$ single crystals. In addition, we examined variations in the electronic structure along the principal axes of monoclinic W:$BiVO_4$. Thus, we shed further light on structural driving forces related to the materials carrier mobility and earlier observations of conductivity anisotropy. XAS and PES indicate that W is in the 6+ oxidation state and substitutes for V^{5+} sites in $BiVO_4$. Valence band PES data show the presence of inter-band gap states upon W doping or the possible creation

of oxygen vacancies. Resonant PES verified that the feature arises from electron states at V^{4+} sites of *e* symmetry, consistent with DFT predictions of small-polarons localising in V $3d_z^2$ states. The energetic position of the state in the gap suggests that the electrons are highly localised. V *L*-/O *K*-edge polarization dependent XAS verified the anisotropy in the electronic structure between the *ab*-plane and *c*-axis. Spectra revealed the improved hybridization of V 3*d*-O 2*p* states and broader conduction bands in the *ab*-plane relative to the *c*-axis. These insights into the electronic structure of $BiVO_4$ may guide the development and optimization of this material for PEC applications.

ACKNOWLEDGEMENTS: The Boston University program is supported by the Department of Energy under Grant No. DE-FG02-98ER45680. The Advanced Light Source is supported by the U.S. Department of Energy under Contract No. DE-AC02-05CH11231. AJER and CBM gratefully acknowledge the U.S. Department of Energy Office of Basic Energy Sciences Grant DE-FG02-09ER16119 and Welch Foundation Grant F-1436. Additionally, AJER acknowledges the Hemphill-Gilmore Endowed fellowship for financial support. J-SZ was supported by NSF MIRT DMR 1122603. VJ would like to thank the beamline scientists at beamlines 8.0.1 and 11.0.2 of the ALS for their assistance during measurements. Beamline 11.0.2 is also supported by the Director, Office of Science, Office of Basic Energy Sciences, and by the Division of Chemical Sciences, Geosciences, and Biosciences of the US Department of Energy at the Lawrence Berkeley National Laboratory under Contract No. DEAC02-05CH11231.

REFERENCES

(1) Z. Li, W. Luo, M. Zhang, J. Feng, Z. Zou. *Energy Environ. Sci.*, 2013, **6**, 347–370.

(2) Y. Park, K. J. McDonald, K.-S. Choi, *Chem. Soc. Rev.*, 2013, **42**, 2321–2337.

(3) W. Luo, Z. Yang, Z. Li, J. Zhang, J. Liu, Z. Zhao, Z. Wang, S. Yan, T. Yu, Z. Zou, *Energy Environ. Sci.*, 2011, **4**, 4046-4051.

(4) Y. Liang, T. Tsubota, L. P. Mooij, R. van de Krol, *J. Phys. Chem. C*, 2011, **115**, 17594–17598.

(5) F. F. Abdi, L. Han, A. H. M. Smets, M. Zeman, B. Dam, R. van de Krol, *Nat. Commun.*, 2013, **4**, 1–7.

(6) A. J. E. Rettie, H. C. Lee, L. G. Marshall, J. F. Lin, C. Capan, J. Lindemuth, J. S. McCloy, J. Zhou, A. J. Bard, C. B. Mullins, *J. Am. Chem. Soc.*, 2013, **135**, 11389–11396.

(7) K. E. Kweon, G. S. Hwang, J. Kim, S. Kim, S. Kim, *Phys. Chem. Chem. Phys.*, 2015, **17**, 256–260.

(8) A. J. E. Rettie, W. D. Chemelewski, J. Lindemuth, J. S. McCloy, L. G. Marshall, J. Zhou, D. Emin, C. B. Mullins, *Appl. Phys. Lett.*, 2015, **106**, 022106.

(9) F. F. Abdi, T. J. Savenije, M. M. May, B. Dam, R. van de Krol. *J. Phys. Chem. Lett.*, 2013, **4**, 2752–2757.

(10) T. Liu, X. Zhou, M. Dupuis, C. Li, *Phys. Chem. Chem. Phys.* 2015, **17**, 23503–23510.

(11) V. Jovic, J. Laverock, A. J. E. Rettie, J. Zhou, C. B. Mullins, V. R. Singh, B. Lamoureux, D. Wilson, T.-Y. Su, B. Jovic, H. Bluhm, T. Söhnel, K. E. Smith, *J. Mater. Chem. A*, 2015, **3**, 23743–23753.

(12) F. D. Ogletree, H. Bluhm, E. B. Hebenstreit, M. Salmeron, *Nucl. Instruments Methods Phys. Res. A*, 2009, **609**, 151–160.

(13) H. Bluhm, K. Andersson, T. Araki, K. Benzerara, G. E. Brown, J. J. Dynes, S. Ghosal,; M. K. Gilles, H. Hansen, J. C. Hemminger, A. P. Hitchcock, G. Ketteler, A. L. D. Kilcoyne, E. Kneedler, J. R. Lawrence, G. G. Leppard, J. Majzlam, B. S. Mun, S. C. B. Myneni, A. Nilsson, H. Ogasawara, D. F. Ogletree, K. Pecher, M. Salmeron, D. K. Shuh, B. Tonner, T. Tyliszczak, T. Warwick, T. H. Yoon, *J. Electron. Spectrosc. Relat. Phenom.*, 2006, **150**, 86–104.

(14) K. E. Kweon, G. S. Hwang, *Phys. Rev. B*, 2012, **86**, 165209.

(15) D. J. Payne, M. D. M. Robinson, R. G. Egdell, A. Walsh, J. McNulty, K. E. Smith, L. F. J. Piper, *Appl. Phys. Lett.*, 2011, **98**, 212110.

(16) A. J. E. Rettie, W. D. Chemelewski, D. Emin, C. B. Mullins, *J. Phys. Chem. Lett.* 2016, **7**, 471-479.

(17) K. E. Kweon, G. S. Hwang, *Phys. Rev. B*, 2013, **87**, 205202.

(18) J. Jaćimović, C. Vaju, A. Magrez, H. Berger, L. Forro, R. Gaal, V. Cerovski, and R. Žikić, *Europhys. Lett.*, 2012, **99**, 57005.

(19) S. Moser, L. Moreschini, J. Jaćimović, O. S. Barišić, H. Berger, A. Magrez, Y. J. Chang, K. S. Kim, A. Bostwick, E. Rotenberg, L. Forro, M. Grioni, *Phys. Rev. Lett*. 2013,**110**, 196403.

(20) Z. A. Feng, F. El Gabaly, X. Ye, Z.-X. Shen, W. C. Chueh, *Nat. Commun.*, 2014, **5**, 1–9.

(21) D. Wu, H. Zhu, C. Zhang, L. Chen, *Chem. Commun.*, 2010, **46**, 7250–7252.

(22) K. P. S. Parmar, H. J. Kang, A. Bist, P. Dua, J. S. Jang, J. S. Lee, *ChemSusChem.*, 2012, **5**, 1926–1934.

(23) K. Ding, B. Chen, Z. Fang, Y. Zhang, Z. Chen, *Phys. Chem. Chem. Phys.*, 2014, **16**, 13465.

(24) L. Lajaunie, F. Boucher, R. Dessapt, P. Moreau, *Ultramicroscopy*, 2014, **149**, 1–8.

(25) G. Wu, T. Sekiguchi, Y. Baba, I. Shimoyama, *Nucl. Instruments Methods Phys. Res. Sect. B Beam Interact. with Mater. Atoms*, 2006, **245**, 406–410.

(26) M. Sing, R. Neudert, H. von Lips, M. Golden, M. Knupfer, J. Fink, R. Claessen, J. Mucke, H. Schmitt, S. Hufner, B. Lommel, W. Assmus, C. Jung, C. Hellwig, *Phys. Rev. B*, 1999, **60**, 8559–8568.

(27) Y. Choi, H. Chang, B.-H. Ryu, K. Kong, J. Do. Lee, K. No, *Jpn. J. Appl. Phys.*, 2003, **42**, 7570–7573.

(28) B. Pattengale, J. Ludwig, J. Huang, *J. Phys. Chem. C*, 2016, **120**, 1421−1427.

(29) J. Laverock, B. Chen, A.R.H. Preston, K.E. Smith, N.R. Wilson, G. Balakrishnan, P.-A. Glans, J.-H. Guo, *Phys. Rev. B*, 2013, **87**, 125133

(30) J. K. Cooper, S. Gul, F. M. Toma, L. Chen, P.-A. Glans, J. Guo, J. W. Ager, J. Yano, I. D. Sharp, *Chem. Mater.*, 2014, **26**, 5365–5373.

(31) U. Bergmann, P. Glatzel, *Photosynth. Res.* 2009, **102**, 255-266.

(32) L. J.P. Ament, M. van Veenendaal, T. P. Devereaux, J. P. Hill, J. van den Brink, *Rev. Mod. Phys.*, 2011, **83**, 0034-6861.